ORIGINAL ARTICLE

High-accuracy prediction of axillary lymph node metastasis in invasive lobular carcinoma using focal cortical thickening on magnetic resonance imaging

Shun Kawaguchi[1] · Keiichi Kinowaki[2] · Nobuko Tamura[1] · Tomohiko Masumoto[3] · Aya Nishikawa[1] · Akio Shibata[1] · Kiyo Tanaka[1] · Yoko Kobayashi[1] · Takuya Ogura[1] · Junichiro Sato[2] · Hidetaka Kawabata[1]

Abstract

Background Invasive lobular carcinoma (ILC) grows diffusely in a single-cell fashion, sometimes presenting only subtle changes in preoperative imaging; therefore, axillary lymph node (ALN) metastases of ILC are difficult to detect using magnetic resonance imaging (MRI). Preoperative underestimation of nodal burden occurs more frequently in ILC than in invasive ductal carcinoma (IDC), however, the morphological assessment for metastatic ALNs of ILC have not fully been investigated. We hypothesized that the high false-negative rate in ILC is caused by the discrepancy in the MRI findings of ALN metastases between ILC and IDC and aimed to identify the MRI finding with a strong correlation with ALN metastasis of ILC.

Method This retrospective analysis included 120 female patients (mean ± standard deviation age, $57.2 ± 11.2$ years) who underwent upfront surgery for ILC at a single center between April 2011 and June 2022. Of the 120 patients, 35 (29%) had ALN metastasis. Using logistic regression, we constructed prediction models based on MRI findings: primary tumor size, focal cortical thickening (FCT), cortical thickness, long-axis diameter (LAD), and loss of hilum (LOH).

Results The area under the curves were 0.917 (95% confidence interval [CI] 0.869–0.968), 0.827 (95% CI 0.758–0.896), 0.754 (95% CI 0.671–0.837), and 0.621 (95% CI 0.531–0.711) for the FCT, cortical thickness, LAD, and LOH models, respectively.

Conclusions FCT may be the most relevant MRI finding for ALN metastasis of ILC, and although its prediction model may lead to less underestimation of the nodal burden, rigorous external validation is required.

Keywords Lymph nodes · Carcinoma · Lobular · Clinical decision-making · Magnetic resonance imaging

Introduction

Breast cancer is a major cause of cancer-related deaths in women. Despite advances in treatment and diagnostic techniques, breast cancer accounted for approximately 680,000 deaths in 2020 worldwide [1]. Metastatic breast cancer is responsible for most cancer-related deaths and spreads to other body sites through the bloodstream and lymphatics. Accurate axillary nodal staging is clinically important because it reflects disease progression at diagnosis and helps determine the optimal treatment intensity. Magnetic resonance imaging (MRI) and ultrasonography (US) are frequently used for nodal evaluation in clinical settings; however, MRI has better diagnostic accuracy than US because US is highly operator-dependent [2].

Invasive lobular carcinoma (ILC) is the most common special subtype of breast cancer, accounting for 10–15% of all breast cancer cases [3]. ILC is characterized by E-cadherin loss, which is crucial in cell–cell adhesion, and typically shows small and non-cohesive epithelial cells dispersed individually. Its clinical presentation differs from that of invasive ductal carcinoma (IDC); Chung et al. reported a different morphology of axillary lymph node (ALN) metastasis for ILC from that of IDC on US [4]. ILC has subtle

✉ Shun Kawaguchi
  kshun51@gmail.com

1 Department of Breast and Endocrinology Surgery, Toranomon Hospital, 2-2-2 Toranomon, Minato City, Tokyo 105-8470, Japan

2 Department of Pathology, Toranomon Hospital, Tokyo, Japan

3 Department of Diagnostic Radiology, Toranomon Hospital, Tokyo, Japan

imaging findings both on mammography and US because ILC frequently appears with a mass density that is less than or equal to that of normal fibroglandular breast tissue on a mammograph, and sometimes shows only a slight architectural distortion on US. Therefore, MRI is recommended to evaluate tumor extent [5]. We hypothesized that a distinct MRI interpretation may be necessary to predict ILC nodal staging; however, the clinical evidence is limited.

We aimed to identify a specific imaging feature of MRI that is highly associated with ALN metastasis of ILC. Based on the previously reported findings [6–8], in this study, we investigated the imaging features correlated with lymph node metastasis for the nodal ILC. We then constructed a logistic regression model and evaluated its diagnostic accuracy using receiver operating characteristic (ROC) analysis.

Material and methods

Patients

From a hospital breast cancer registry in Japan, we retrospectively identified 169 Asian women diagnosed with ILC via core needle biopsy between April 2011 and June 2022. The exclusion criteria included the absence of MRI data (n = 32), neoadjuvant chemotherapy history (n = 13), neoadjuvant endocrine therapy history (n = 3), and coronavirus disease vaccination 6 months prior (n = 1). Overall, 120 women were eligible and randomized to the derivation cohort (Fig. 1). Tumor and nodal stages were allocated according to the Tumor–Node–Metastasis (TNM) staging system proposed by the American Joint Committee on Cancer, 8th edition [9].

Fig. 1 Study design. **a** Patient enrolment flowchart. The chart shows the screening of 169 patients who underwent breast surgeries for primary invasive lobular carcinoma in our hospital between April 2011 and June 2022. **b** The steps of data analysis. *ALN* axillary lymph node, *ET* endocrine therapy, *ILC* invasive lobular carcinoma, *MRI* magnetic resonance imaging, *NAC* neoadjuvant chemotherapy
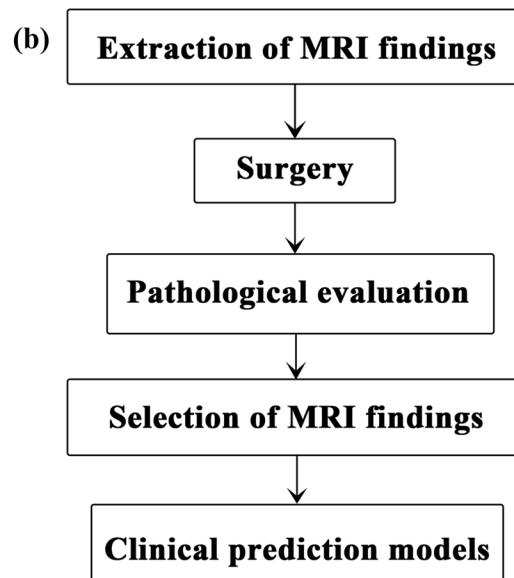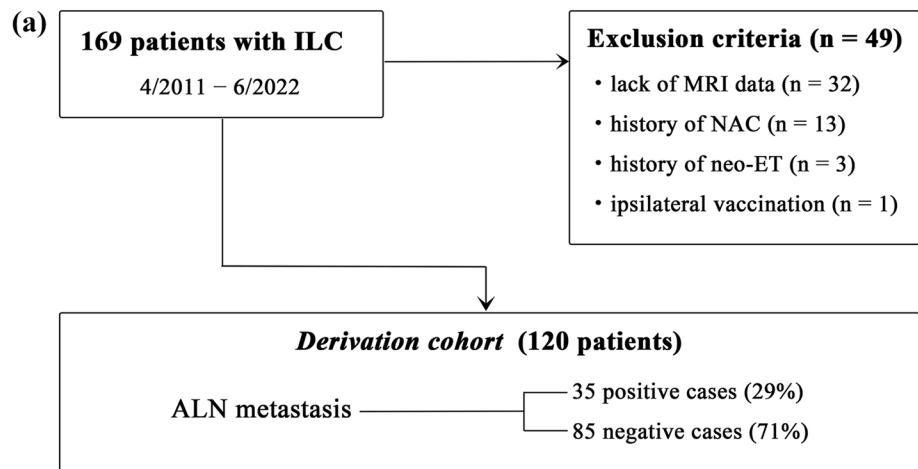
The relevant ethics committee approved the study protocol (registration number: 1552). Since the study was retrospective and anonymous, the requirement for informed consent was waived.

Imaging protocol

We used a 3.0-Tesla (T) MRI to assess the nodal staging and tumor extension of primary breast cancer with patients in the prone position, with their arms laid down. At our institution, dynamic contrast-enhanced MRI was performed using a 3.0-Tesla (T) MRI scanner (Ingenia, Philips Healthcare, Best, The Netherlands) with seven-channel breast coils. T1-weighted imaging (TR/TE, 640/10 ms; phase encoding direction, right-to-left; flip angle, 90º; field of view, 320 × 320 mm, thickness, 3 mm; matrix, 304 × 384) and T2-weighted imaging with fat suppression (TR/TE, 10,700/80 ms; phase encoding direction, right-to-left; flip angle, 80°; field of view, 320 × 320 mm, thickness, 3 mm; matrix, 288 × 288) were obtained as one pre-contrast imaging. After intravenous administration of gadoteridol (Prohance, Bracco, Milan, Italy) using a single dose of 0.1 mmol/kg body weight at a flow rate of 3 ml/s, dynamic contrast-enhanced, fat-suppressed, gradient echo, and T1-weighted axial imaging (TR/TE, 3.8/1.95 ms; phase encoding direction, right-to-left; flip angle, 12°; field of view, 320 × 320 mm; thickness, 2 mm; matrix, 352 × 384) was performed. Sequential acquisitions of the four post-contrast images were obtained at 60 s, 120 s, 180 s, and 360 s.

Imaging analysis

The images or standardized reports of imaging findings of ALNs were collected from the electronic medical records. Morphological evaluation was performed according to criteria from previous reports [10]. Breast and axillary MR images were retrospectively reviewed; the readers were blinded to the clinical information regarding ALN analysis during radiogram interpretation. Two readers (S.K. and H.K. [breast surgeons with 5 and > 20 years of experience, respectively]) separately performed image analysis. When disagreements occurred, the third reader, an experienced radiologist (T.M.) with > 20 years of experience in MRI interpretation, was consulted. In the interpretation session, all detectable ALNs at least 3 mm in long-axis diameter were measured on both sides. Four images were obtained at 60 s, 120 s, 180 s, and 360 s in the post-contrast phase of the T1-weighted axial imaging when the primary lesion and ALNs were most clearly visualized, and the following were recorded: maximum long-axis diameter (LAD), maximum cortical thickness, the presence of focal cortical thickening (FCT) (Fig. 2), and the presence of loss of hilum (LOH). The maximum cortical thickness was measured perpendicular

to the long axis of the ALNs in a transverse direction. FCT was defined as non-uniform cortical thickening showing single or multiple bulges protruding from the lymph node cortex. When LOH was suspected, the short-axis diameter was substituted for the cortical thickness. LOH was judged as positive only when the short-axis diameter was ≥ 4 mm on MRI [11]. When LOH or FCT was observed, the lymph node data presenting such features were selected.

Axillary surgery

Sentinel lymph node biopsy was performed using the dual method with phytate sodium hydrate, technetium-phytic acid, and indigo carmine. The sentinel lymph nodes were frozen, sectioned at a thickness of 2 mm, and sent to expert pathologists to determine whether they contained cancer cells. Based on the quick examination of sentinel lymph node results, we performed or omitted ALN sampling or ALN dissection to level I/II based on the case corresponding to the ACOSOG Z0011 trial [12].

Pathological evaluation

Tissue specimens were obtained through preoperative core needle or vacuum-assisted biopsies. The detailed pathological evaluations are described in the Supplementary Material (online).

Statistical analysis

Numeric data are expressed as mean ± standard deviation (SD). Continuous variables were compared between the two groups using the Student's t-test. The optimal cut-off values for Ki-67, tumor size, LAD, cortical thickness, and FCT were determined using ROC analysis based on the Youden index. We first identified significant factors ($p < 0.05$) associated with ALN metastasis in a univariate analysis using Fisher's exact test. Then, the diagnostic accuracy was assessed using the AUC values of the logistic regression models. The percentage FCT agreement was evaluated using kappa statistics. Statistical analyses were performed using R: a language and environment for statistical computing version, 4.0.3 (R Foundation for Statistical Computing, Vienna, Austria). A p-value lower than 0.05 was accepted as the significance level for all analyses.

Results

Of the 120 female patients with ILC (mean ± SD age, 57.2 ± 11.2 years) in the derivation cohort, 35 (29%) had ALN metastases. Primary ILC exhibited a T category of T1 in 56% (67/120), T2 in 33% (40/120), and T3 in 11%

Fig. 2 Representative images of a 60-year-old female patient with ALN metastasis of invasive lobular carcinoma (pT1c-N1aM0, pStage IIA; Luminal B-like type). **a** Transverse contrast-enhanced T1-weighted magnetic resonance image showing an enlarged axillary lymph node in level I, presenting FCT (red arrow). **b** Panoramic-view metastatic ALN image showing eccentric FCT of the nodular metastatic foci. **c** Solid components consisting of discohesive tumor cells with round nuclei (grade 2 nuclear score) within the metastatic ALN (hematoxylin and eosin staining; [**b**]×20, [**c**]×200). *ALN* axillary lymph node, *FCT* focal cortical thickening
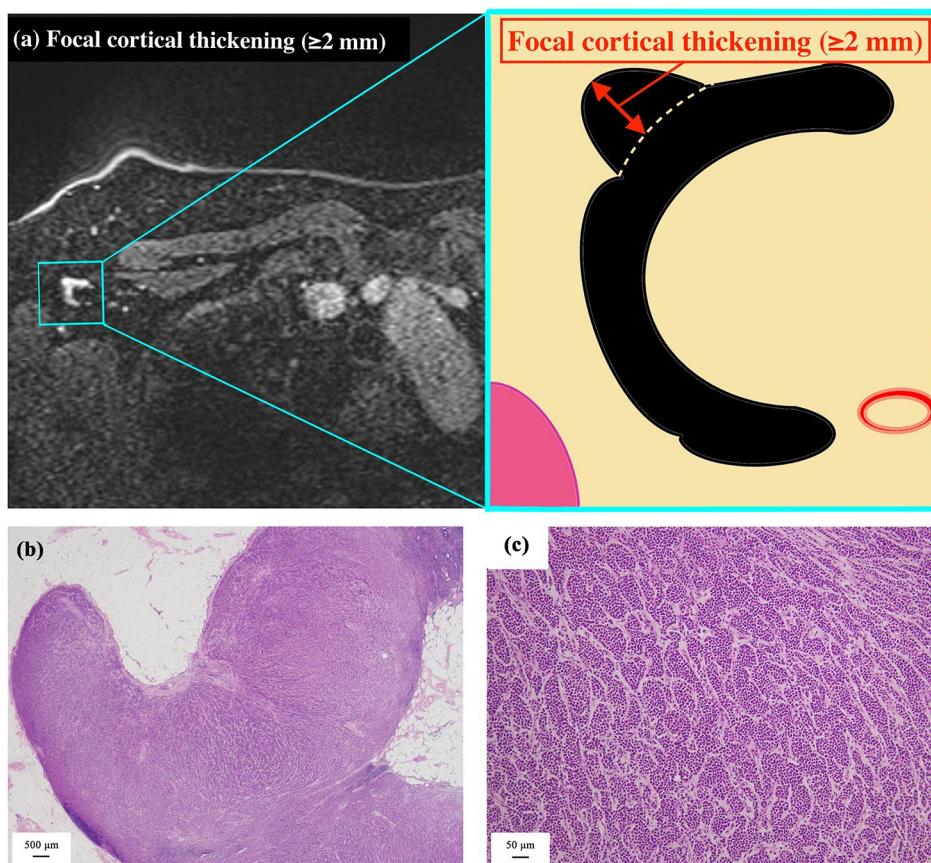
(13/120), and an N category of N1mi in 3% (3/120), N1a in 18% (21/120), N2a in 6% (7/120), and N3a in 3% (4/120). The pathological TNM stage was IA in 43% (52/120), IB in 1% (1/120), IIA in 33% (40/120), IIB in 10% (12/120), IIIA in 9% (11/120), and IIIC in 3% (4/120) of the patients.

Table 1 summarizes the patient characteristics and statistical comparisons between the two groups with or without ALN metastasis in the derivation cohort. Pathological tumor size and histological grade were significantly greater in patients with ALN metastasis ($p < 0.05$). The cut-off value of cortical thickness change defining 'FCT-positive' was identified as 2 mm at the level with the highest area under the curve (AUC) value by ROC analysis as in Fig. 3. In the derivation cohort, FCT and LOH were present in 41 (34%) and 23 (19%) patients on MRI, respectively. Of the 35 patients who had ALN metastasis, 32 (91%) and 6 (17%) patients had FCT and LOH on MRI, respectively. Micrometastases (lesion ≤ 2 mm) were seen in only two patients. The average lymph node size on MRI and percentage of patients with FCT were significantly higher in patients with ALN metastasis than in patients without ALN metastasis ($p < 0.05$).

ROC analysis determined optimal cut-off values for Ki-67 grade (≥ 10% vs. < 10%), MRI tumor size (≥ 14 vs. < 14 mm), LAD (≥ 8 vs. < 8 mm), cortical thickness (≥ 4 vs. < 4 mm), and FCT (≥ 2 vs. < 2 mm) (Fig. 3). Table 2 shows the univariate analysis results of each predictor and clinical prediction models established by logistic regression in the derivation cohort. Of the five MRI findings, LOH was not significantly associated with ALN metastasis ($p > 0.05$). The FCT model had significantly better diagnostic accuracy (AUC = 0.917; 95% confidence interval [CI] 0.869–0.966) than any other model in the derivation cohort ($p < 0.05$). The cortical thickness model showed the second-best diagnostic performance (AUC = 0.827; 95% CI 0.758–0.896), while the other two models' AUCs were both below 0.800.

Table 3 demonstrates the sensitivity, specificity, positive predictive value (PPV), negative predictive value, and false-negative rate of each predictor on MRI. Of the four prediction models, the MRI FCT model showed the lowest false-negative rate (9%, 3/35). The percentage agreement of FCT on MRI among the 120 cases categorized by two interpreters was 87.5% (105/120), with a kappa coefficient of 0.73 (95% CI 0.60–0.86).

Table 1 Characteristics of the patients with or without axillary lymph node metastasis

Characteristics	Metastasis (−) (n=85) (%)	Metastasis (+) (n=35) (%)	p-value
Age, years (mean)±SD	58.2±11.2	54.6±10.9	0.15
Histopathologic findings			
Histological grade			0.018
I	12 (14)	0 (0)	
II	72 (85)	34 (97)	
III	1 (1)	1 (3)	
Nuclear grade			0.83
1	69 (81)	27 (77)	
2	14 (16)	7 (20)	
3	2 (2)	1 (3)	
Ki-67 grade			0.36
<20%	66 (78)	24 (69)	
≥20%	19 (22)	11 (31)	
Lymphovascular invasion			<0.001
Absent	75 (88)	14 (40)	
Present	10 (12)	21 (60)	
Tumor size on pathological examination[a] (mm)	22.3±18.4	36.2±27.6	0.0038
Molecular subtypes			0.46
Luminal A-like (Ki-67<20%)	44 (52)	20 (57)	
Luminal B-like (Ki-67≥20%)	36 (42)	13 (37)	
Luminal-HER2	2 (2)	1 (3)	
Pure HER2	0 (0)	1 (3)	
Triple-negative	3 (4)	0 (0)	
MRI findings			
Tumor size[a] (mm)	21.9±14.2	24.7±13.5	0.12
Lymph node size[a] (mm)			
Long-axis diameter	9.0±4.2	11.8±4.5	0.0052
Cortical thickness	2.9±1.2	5.5±3.0	<0.001
Focal cortical thickening			<0.001
Negative (cortical thickness change<2 mm)	76 (89)	3 (9)	
Positive (cortical thickness change≥2 mm)	9 (11)	32 (91)	
Loss of hilum			0.80
Negative	68 (80)	29 (83)	
Positive	17 (20)	6 (17)	

*SD* standard deviation, *HER2* human epidermal growth factor receptor 2, *MRI* agnetic resonance imaging

[a]Data represent means±SDs

Discussion

In our study, FCT of ALNs was an independent predictive factor for ALN metastasis of ILC, and the MRI FCT model had the highest accuracy. The new high-sensitivity approach to nodal staging of patients with ILC using MRI FCT may lead to a more accurate nodal burden estimation.

Extensive radiologic research has been conducted to achieve high-accuracy nodal staging in patients with breast cancer [13–17]. Unlike IDC, positron emission tomography/computed tomography is not suitable for nodal staging of ILC because ILC has a lower conspicuity [15]. Of several diagnostic accuracy studies showing detailed ALN morphological features, Kim et al. demonstrated that the cortical thickness-derived parameters (eccentricity, irregularity and LOH of ALNs) were significantly associated with ALN metastasis [17]. However, ILC accounted for less than 5% of cases in the study cohort; therefore, the predictive ability of those parameters for ALN metastasis in patients with ILC has not been fully investigated. Furthermore, the cut-off value of the morphological features of metastatic ALNs was not well-established in the previous literature [11, 13, 18]. In our experience [19], the presence of LOH caused by metastasis cannot be judged when ALNs are smaller than 4 mm in

ROC curves of the FCT models with the different threshold standards
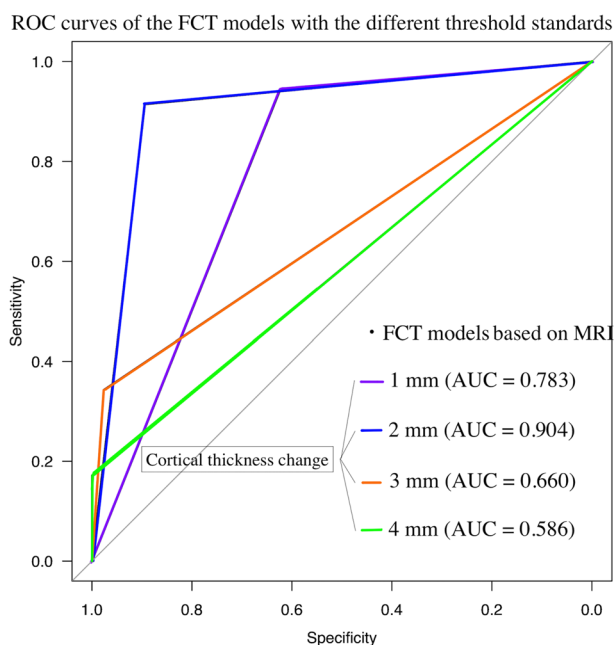
Fig. 3 ROC curves of the clinical prediction models based on the different threshold standards of FCT on MRI, ranging from 1 to 4 mm. The FCT model of 2 mm showed the better AUC of 0.904 (95% confidence interval [CI] 0.847–0.962) than any other model; 0.783 (95% CI 0.718–0.848) of the 1-mm model, 0.660 (95% CI 0.578–0.741) of the 3-mm model, and 0.586 (95% CI 0.522–0.649) of the 4-mm model. *AUC* area under the curve, *FCT* focal cortical thickening, *MRI* magnetic resonance imaging, *ROC* receiver operating characteristic

long-axis diameter. Moreover, as most normal ALNs smaller than 4 mm show a round shape, we measured all ALNs that were at least 3 mm in long-axis diameter, and tried to interpret the cortex structure as closely as possible.

The finding of LOH, namely the 'hilar mass effect' on US, is reportedly caused by the expansive growth of nodular metastatic foci into the fatty sinusoid space and has been widely accepted as a typical metastatic lymph node finding [20, 21]. However, in our analysis, LOH was not detected in 73% of metastatic ALNs in ILC. Similarly, a recent retrospective study showed that the metastatic ALN exhibited diffuse cortical thickening without a hilar mass effect on US in 68.9% of patients with ILC vs. 28.8% of patients with IDC [4]. The detailed molecular mechanism of this difference is unclear; however, considering that nodular metastatic patterns were observed in approximately the same proportion (approximately 70%) of node-positive IDCs and ILCs on histopathologic examination [22], an expansive growth into the sinusoid by nodular metastatic foci might be less likely to occur in ILC than in IDC due to ILC non-cohesive and migratory properties. This discrepancy in metastatic patterns between IDC and ILC may contribute to the highly sensitive MRI detection of ALN metastasis of ILC. In IDC, it is difficult to recognize the changes in cortical contour

and thickness in detail because LOH is frequently detected in the metastatic ALNs of these patients, and lymph nodes with LOH are visualized as round or oval homogeneous hyperintense lesions on T1-weighted MRI in clinical practice [23]. Unfortunately, LOH is also observed in reactive lymph nodes; therefore, it may contribute to false-positive results. Additionally, the difference in the prevalence rate of the LOH metastatic pattern in ALNs between IDC and ILC may be one of the factors influencing the false-positive result of the two subtypes in breast MRI findings.

FCT finding, which is non-uniform cortical thickening showing single or multiple bulges, is the key feature of this analysis. It had the highest sensitivity (88%) and specificity (91%) for ALN metastasis of ILC among all predictors. FCT is caused by scattered metastatic foci in the cortex and is either concentric or eccentric. Paish et al. previously demonstrated that the metastatic growth in the lymph nodes of patients with breast cancer was divided into three patterns: nodular, diffuse, and sinusoidal [23]. The FCT can be masked only when the sinusoidal pattern is predominant because nodular and diffuse patterns are both likely to show an apparent morphological change in the cortex of ALNs, such as FCT. A previous retrospective study that compared the proportions of metastatic growth patterns between IDC and ILC revealed that no metastatic ALN exhibited a sinusoidal pattern in 27 patients with ILC [22]. The high diagnostic accuracy of the FCT model that we used in our analysis may be attributed to this distinct metastatic growth pattern in the lymph nodes of patients with ILC.

Here, nodal FCT-oriented MRI assessment achieved higher accuracy and a drastically lower false-negative rate than in a previous study [24–26]. In previous studies, the positive diagnostic criteria of metastatic ALNs in ILC using MRI and US have included both LOH imaging features and cortical thickness as they were used in IDC. To our knowledge, the cortical thickness change of ALNs in ILC has not been investigated in detail. In our analysis, using ROC analysis, FCT was defined as ALN with a cortical thickness change ≥ 2 mm; this may be the most important MRI finding for predicting ALN metastasis of ILC, and the detailed information of cut-off value was not previously reported in literature. Our findings may have important implications for axillary ILC management in clinical settings. Previous studies have reported that ILC is subtle on preoperative imaging, and that metastatic ALNs of ILC are fewer and smaller than those of IDC [4, 24]. Based on our results, by carefully observing the changes in cortical thickness and contour during MRI interpretation, false-negative results may be reduced. If FCT is present on MRI, a second-look US and sequential ALN biopsy targeting FCT should be performed to avoid underestimating nodal burden. This information is helpful for most clinicians, including surgeons, oncologists, and pathologists, since missing locally advanced cancer may

Table 2 Predictors of axillary lymph node metastasis in four clinical predictive models based on magnetic resonance imaging

Predictors	Univariate analysis; p-value	MRI LAD model			MRI cortical thickness model			MRI FCT model			MRI LOH model		
		β (SD)	OR (95% CI)	p-value	β (SD)	OR (95% CI)	p-value	β (SD)	OR (95% CI)	p-value	β (SD)	OR (95% CI)	p-value
Histopathological findings													
Ki-67 grade (≥10% vs. <10%)	0.31												
ER status (positive vs. negative)	0.72												
PR status (positive vs. negative)	0.032*												
Molecular subtype (luminal A vs. non-luminal A)	0.69												
MRI findings													
Primary tumor size (≥14 vs. <14 mm)	0.022*	1.4 (0.6)	4.0 (1.2–13.1)	0.022*	1.0 (0.7)	2.8 (0.8–10.2)	0.11	0.7 (0.8)	1.9 (0.4–9.9)	0.44	1.3 (0.6)	3.8 (1.2–11.9)	0.021*
Axillary lymph node morphology													
Long-axis diameter (≥8 vs. <8 mm)	<0.001*	2.1 (0.6)	8.2 (2.6–25.5)	<0.001*									
Cortical thickness (≥4 vs. <4 mm)	<0.001*				2.7 (0.5)	14.4 (5.2–40.1)	<0.001*						
Focal cortical thickening (positive vs. negative)	<0.001*							4.4 (0.7)	82.3 (20.8–326)	<0.001*			
Loss of hilum (positive vs. negative)	0.80										−0.2 (0.5)	0.8 (0.3–2.3)	0.70
AUC		0.754 (95% CI 0.671–0.837)			0.827 (95% CI 0.758–0.896)			0.917 (95% CI 0.869–0.966)			0.621 (95% CI 0.531–0.711)		0.692

β β coefficients, *SD* standard deviation, *OR* odds ratio, *CI* confidence interval, *LAD* long-axis diameter, *FCT* focal cortical thickening, *LOH* loss of hilum, *ER* estrogen receptor, *PR* progesterone receptor, *MRI* magnetic resonance imaging, *AUC* area under the curve

*Significant p-value (p < 0.05)

Table 3 Diagnostic performance of each predictor of magnetic resonance imaging

Predictor	Sensitivity	Specificity	Positive predictive value	Negative predictive value	False-negative rate
MRI findings					
Primary tumor size (≥ 14 vs. < 14 mm)	89% (31/35)	33% (28/85)	35% (31/88)	88% (28/32)	11% (4/35)
Long-axis diameter of ALN (≥ 8 vs. < 8 mm)	89% (31/35)	51% (43/85)	42% (31/73)	91% (43/47)	11% (4/35)
Cortical thickness of ALN (≥ 4 vs. < 4 mm)	91% (32/35)	76% (65/85)	62% (32/52)	96% (65/68)	9% (3/35)
Focal cortical thickening of ALN (positive vs. negative)	91% (32/35)	89% (76/85)	78% (32/41)	96% (76/79)	9% (3/35)
Loss of hilum of ALN (positive vs. negative)	17% (6/35)	80% (68/85)	26% (6/23)	70% (68/97)	83% (29/35)

MRI magnetic resonance imaging, *ALN* axillary lymph node

result in poor clinical outcomes, and ILC histology is associated with a significantly frequent underestimation of the nodal burden in surgical pathology [27].

Accurate nodal staging might improve the clinical outcome of patients with ILC by reducing the undertreatment; however, the literature on the benefits of neoadjuvant chemotherapy for node-positive ILCs is conflicting [28–30]. Considering that most ILCs are luminal A-like type tumors with low histological grades and mitotic activities, a poorer response to neoadjuvant chemotherapy than IDCs seems biologically plausible [31]. Endocrine therapy generally shows lower rates of serious adverse events than chemotherapy, whereas the overall survival benefit of neoadjuvant endocrine therapy for patients with node-positive ILC was reported to be non-inferior to that of neoadjuvant chemotherapy [32]. Although the treatment benefit of neoadjuvant systemic therapy may be limited for ILC, accurate nodal upstaging before surgery can expand treatment options. For example, neoadjuvant therapy may be safely followed with sentinel lymph node biopsy [33] or omission of ALN dissection in certain populations [34].

Our study had several limitations. Firstly, this was a single-institution retrospective study with a small sample size, and the findings should be externally validated in future analyses. Secondly, the number of patients with human epidermal growth factor receptor 2-positive or triple-negative breast cancers was very small due to the history of neoadjuvant chemotherapy, which makes it difficult to directly compare pathological findings with imaging findings. Thirdly, we could not ensure that the surgically resected ALNs showed specific features such as FCT or LOH, because the only preoperative marking techniques for the ALNs used were the radioisotope and dyeing methods for sentinel lymph node biopsy. Finally, in a clinical setting, US-guided fine-needle aspiration is frequently performed to get the pathological diagnosis before operation. Therefore, future prospective, comparative diagnostic test accuracy studies focusing on US FCT are needed to make MRI FCT more clinically useful.

In conclusion, our MRI-detected FCT-focused clinical prediction model demonstrated an excellent diagnostic accuracy for ALN metastases of ILC. In MRI interpretation, close observation of the contour and thickness change of the cortex is important to avoid underestimation of the nodal burden in patients with ILC; however, further external validation studies in clinical settings are required.

Declarations

Ethical approval The relevant ethics committee approved the study protocol (registration number: 1552).

Informed consent For this type of study formal consent is not required.

References

1. Sung H, Ferlay J, Siegel RL, Laversanne M, Soerjomataram I, Jemal A, et al. Global cancer statistics 2020: GLOBOCAN estimates of incidence and mortality worldwide for 36 cancers in 185 countries. CA Cancer J Clin. 2021;71:209–49.

2. Marino MA, Avendano D, Zapata P, Riedl CC, Pinker K. Lymph node imaging in patients with primary breast cancer: concurrent diagnostic tools. Oncologist. 2020;25:e231–42.

3. McCart Reed AE, Kalinowski L, Simpson PT, Lakhani SR. Invasive lobular carcinoma of the breast: the increasing importance of this special subtype. Breast Cancer Res. 2021;23:6.

4. Chung HL, Tso HH, Middleton LP, Sun J, Leung JWT. Axillary nodal metastases in invasive lobular carcinoma versus invasive ductal carcinoma: comparison of node detection and morphology by ultrasound. AJR Am J Roentgenol. 2022;218:33–41.

5. Mann RM, Hoogeveen YL, Blickman JG, Boetes C. MRI compared to conventional diagnostic work-up in the detection and evaluation of invasive lobular carcinoma of the breast: a review of existing literature. Breast Cancer Res Treat. 2008;107:1–14.

6. Fischerova D, Garganese G, Reina H, Fragomeni SM, Cibula D, Nanka O, et al. Terms, definitions and measurements to describe sonographic features of lymph nodes: consensus opinion from the Vulvar International Tumor Analysis (VITA) group. Ultrasound Obstet Gynecol. 2021;57:861–79.

7. Mortellaro VE, Marshall J, Singer L, Hochwald SN, Chang M, Copeland EM, et al. Magnetic resonance imaging for axillary staging in patients with breast cancer. J Magn Reson Imaging. 2009;30:309–12.

8. Valente SA, Levine GM, Silverstein MJ, Rayhanabad JA, Weng-Grumley JG, Ji L, et al. Accuracy of predicting axillary lymph node positivity by physical examination, mammography, ultrasonography, and magnetic resonance imaging. Ann Surg Oncol. 2012;19:1825–30.

9. Amin MB, Edge SB, Greene FL, Byrd DR, Brookland RK, Washington MK, et al. AJCC cancer staging manual. 8th ed. New York: Springer; 2017.

10. Sung JS, Li J, Da Costa G, Patil S, Van Zee KJ, Dershaw DD, et al. Preoperative breast MRI for early-stage breast cancer: effect on surgical and long-term outcomes. AJR Am J Roentgenol. 2014;202:1376–82.

11. Ha SM, Chae EY, Cha JH, Shin HJ, Choi WJ, Kim HH. Diagnostic performance of standard breast MR imaging compared to dedicated axillary MR imaging in the evaluation of axillary lymph node. BMC Med Imaging. 2020;20:45.

12. Giuliano AE, Ballman KV, McCall L, Beitsch PD, Brennan MB, Kelemen PR, et al. Effect of axillary dissection vs no axillary dissection on 10-year overall survival among women with invasive breast cancer and sentinel node metastasis: the ACOSOG Z0011 (Alliance) randomized clinical trial. JAMA. 2017;318:918–26.

13. Baltzer PA, Dietzel M, Burmeister HP, Zoubi R, Gajda M, Camara O, et al. Application of MR mammography beyond local staging: is there a potential to accurately assess axillary lymph nodes? Evaluation of an extended protocol in an initial prospective study. AJR Am J Roentgenol. 2011;196:W641–7.

14. Topps A, Clay V, Absar M, Howe M, Lim Y, Johnson R, et al. The sensitivity of pre-operative axillary staging in breast cancer: comparison of invasive lobular and ductal carcinoma. Eur J Surg Oncol. 2014;40:813–7.

15. Hogan MP, Goldman DA, Dashevsky B, Riedl CC, Gönen M, Osborne JR, et al. Comparison of 18F-FDG PET/CT for systemic staging of newly diagnosed invasive lobular carcinoma versus invasive ductal carcinoma. J Nucl Med. 2015;56:1674–80.

16. van Nijnatten TJA, Ploumen EH, Schipper RJ, Goorts B, Andriessen EH, Vanwetswinkel S, et al. Routine use of standard breast MRI compared to axillary ultrasound for differentiating between no, limited and advanced axillary nodal disease in newly diagnosed breast cancer patients. Eur J Radiol. 2016;85:2288–94.

17. Kim WH, Kim HJ, Lee SM, Cho SH, Shin KM, Lee SY, et al. Preoperative axillary nodal staging with ultrasound and magnetic resonance imaging: predictive values of quantitative and semantic features. Br J Radiol. 2018;91:20180507.

18. Samiei S, Smidt ML, Vanwetswinkel S, Engelen SME, Schipper RJ, Lobbes MBI, et al. Diagnostic performance of standard breast MRI compared to dedicated axillary MRI for assessment of node-negative and node-positive breast cancer. Eur Radiol. 2020;30:4212–22.

19. Kawaguchi S, Tamura N, Tanaka K, Kobayashi Y, Sato J, Kinowaki K, et al. Clinical prediction model based on 18F-FDG PET/CT plus contrast-enhanced MRI for axillary lymph node macrometastasis. Front Oncol. 2022;12: 989650.

20. Berg WA, Gutierrez L, NessAiver MS, Carter WB, Bhargavan M, Lewis RS, et al. Diagnostic accuracy of mammography, clinical examination, US, and MR imaging in preoperative assessment of breast cancer. Radiology. 2004;233:830–49.

21. Lopez JK, Bassett LW. Invasive lobular carcinoma of the breast: spectrum of mammographic, US, and MR imaging findings. Radiographics. 2009;29:165–76.

22. Fernández B, Paish EC, Green AR, Lee AH, Macmillan RD, Ellis IO, et al. Lymph-node metastases in invasive lobular carcinoma are different from those in ductal carcinoma of the breast. J Clin Pathol. 2011;64:995–1000.

23. Paish EC, Green AR, Rakha EA, Macmillan RD, Maddison JR, Ellis IO. Three-dimensional reconstruction of sentinel lymph nodes with metastatic breast cancer indicates three distinct patterns of tumour growth. J Clin Pathol. 2009;62:617–23.

24. Morrow E, Lannigan A, Doughty J, Litherland J, Mansell J, Stallard S, et al. Population-based study of the sensitivity of axillary ultrasound imaging in the preoperative staging of node-positive invasive lobular carcinoma of the breast. Br J Surg. 2018;105:987–95.

25. Ha SM, Chang JM, Kim SY, Lee SH, Kim ES, Kim YS, et al. Prediction of axillary nodal burden in patients with invasive lobular carcinoma using MRI. Breast Cancer Res Treat. 2021;186:463–73.

26. Schumacher K, Inciardi M, O'Neil M, Wagner JL, Shah I, Amin AL, et al. Is axillary imaging for invasive lobular carcinoma accurate in determining clinical node staging? Breast Cancer Res Treat. 2021;185:567–72.

27. Truin W, Vugts G, Roumen RM, Maaskant-Braat AJ, Nieuwenhuijzen GA, van der Heiden-van der Loo M, et al. Differences in response and surgical management with neoadjuvant chemotherapy in invasive lobular versus ductal breast cancer. Ann Surg Oncol. 2016;23:51–7.

28. Petrelli F, Barni S. Response to neoadjuvant chemotherapy in ductal compared to lobular carcinoma of the breast: a meta-analysis of published trials including 1,764 lobular breast cancer. Breast Cancer Res Treat. 2013;142:227–35.

29. Van Wyhe RD, Caudle AS, Shaitelman SF, Perkins GH, Buchholz TA, Hoffman KE, et al. A component of lobular carcinoma in clinically lymph node-negative patients predicts for an increased likelihood of upstaging to pathologic stage III breast cancer. Adv Radiat Oncol. 2018;3:252–7.

30. O'Connor DJ, Davey MG, Barkley LR, Kerin MJ. Differences in sensitivity to neoadjuvant chemotherapy among invasive lobular and ductal carcinoma of the breast and implications on surgery—a systematic review and meta-analysis. Breast. 2022;61:1–10.

31. Mathieu MC, Rouzier R, Llombart-Cussac A, Sideris L, Koscielny S, Travagli JP, et al. The poor responsiveness of infiltrating lobular breast carcinomas to neoadjuvant chemotherapy can be explained by their biological profile. Eur J Cancer. 2004;40:342–51.

32. Thornton MJ, Williamson HV, Westbrook KE, Greenup RA, Plichta JK, Rosenberger LH, et al. Neoadjuvant endocrine therapy versus neoadjuvant chemotherapy in node-positive invasive lobular carcinoma. Ann Surg Oncol. 2019;26:3166–77.

33. Tsung K, Grobmyer SR, Tu C, Abraham J, Budd GT, Valente SA. Neoadjuvant systemic therapy in invasive lobular breast cancer: is it indicated? Am J Surg. 2018;215:509–12.

34. Boughey JC, Suman VJ, Mittendorf EA, Ahrendt GM, Wilke LG, Taback B, et al. Sentinel lymph node surgery after neoadjuvant chemotherapy in patients with node-positive breast cancer: the ACOSOG Z1071 (Alliance) clinical trial. JAMA. 2013;310:1455–61.